Cellulose (2017) 24:1971–1984
DOI 10.1007/s10570-017-1259-0

ORIGINAL PAPER

Effect of sample moisture content on XRD-estimated cellulose crystallinity index and crystallite size

Umesh P. Agarwal · Sally A. Ralph · Carlos Baez · Richard S. Reiner · Steve P. Verrill

Received: 5 November 2016 / Accepted: 14 March 2017 / Published online: 18 March 2017

Abstract Although X-ray diffraction (XRD) has been the most widely used technique to investigate crystallinity index (CrI) and crystallite size (L_{200}) of cellulose materials, there are not many studies that have taken into account the role of sample moisture on these measurements. The present investigation focuses on a variety of celluloses and cellulose containing materials—from loblolly pine wood to tunicin, and evaluated moisture-induced changes in CrI and L_{200}. It was observed that upon introduction of a small amount of water (5%) into P_2O_5 dried samples, for most samples, both absolute intensity of (200) reflection and its full width at half maximum declined. Moreover, (200) peak position (2θ max) increased when the samples became moist. Although the extent of such changes were material dependent, in general, a greater degree of change was associated with lower sample CrI. For CrI, maximum and minimum increases occurred for oven dried NaOH treated red pine holopulp and tunicin, respectively. For L_{200}, maximum and minimum increases were for wood and tunicin, respectively. Moreover, 2θ max position for (200) reflection increased most for the wood and oven dried NaOH treated red pine holopulp (acid chlorite delignified milled-wood) and least for tunicin. The nonparametric statistical test "sign test" further supported these results. Observations from longer duration drying experiments, post moistening, indicated that the changes to the XRD parameters were reversible to some degree. Based on the findings it is concluded that for most cellulose materials with Segal CrI $< 90\%$ the moisture content has a significant bearing on the XRD-estimated CrI and L_{200} data. Consequently, it is essential that when such materials are compared, their diffractograms should be obtained under similar levels of sample moisture content.

Keywords Cellulose · X-ray diffraction · Crystallinity · Crystallite size · Moisture

Introduction

Because cellulose materials are naturally produced, are renewable and sustainable, they are important commercial feedstocks for a number of industries. Cellulose is a nature made material which is found in abundance, mainly in biomass although it's also produced by some bacteria (Klemm et al. 2011; Tokoh et al. 1998) and sea animal (tunicate, Favier et al. 1995). Several reviews that focused on the field of cellulose have been published (Klemm et al. 2011;

Electronic supplementary material The online version of this article (doi:10.1007/s10570-017-1259-0) contains supplementary material, which is available to authorized users.

U. P. Agarwal (✉) · S. A. Ralph · C. Baez · R. S. Reiner · S. P. Verrill
Forest Products Laboratory, USDA FS, 1 Gifford Pinchot Drive, Madison, WI 53726-2398, USA
e-mail: uagarwal@fs.fed.us

Moon et al. 2011; Zhu et al. 2016). Currently, cellulose materials are objects of vigorous research and development activity for producing renewable energy (Armstrong et al. 2016) and nanomaterials (Eichhorn 2011; Isogai 2013; Zhu et al. 2016). Fuels and chemicals that are derived from cellulose have been getting increased attention (Zhu et al. 2016) due to cellulose being a renewable and environmentally friendly material. Similarly, significant research efforts are focused in areas of materials that incorporate nanocelluloses (Eichhorn 2011; Klemm et al. 2011; Moon et al. 2011; Zhu et al. 2016). In both these fields, understanding of aggregated cellulose at molecular and supramolecular levels is very important because properties, both physicochemical and mechanical, as well as reactivity of cellulose materials are influenced by cellulose structures.

In XRD, depending upon the nature of the sample, not only CrI depends upon the fraction of crystalline material but also is a reflection of crystallite size when latter is varying (French and Santiago Cintrón 2013). XRD has been used to investigate structures of celluloses and cellulose based materials for a long time (Ahvenainen et al. 2016; Nishiyama et al. 2002; Oh et al. 2005; Segal et al. 1959; Sisson 1933). In particular, the technique has been used extensively to calculate both CrI and L_{200}. This is largely due to the X-ray method's availability and simplicity (Park et al. 2010). Certainly, there are other methods available to measure these characteristics. For example, to estimate CrI, NMR (Larsson et al. 1999; Newman 1999; Peciulyte et al. 2015), Raman spectroscopy (Agarwal et al. 2010, 2013, 2014; Schenzel et al. 2005), DSC (Bertran and Dale 1986), sum frequency vibrational spectroscopy (Barnette et al. 2012), terahertz spectroscopy (Vieira and Pasquini 2014), and FT-IR spectroscopy (Hulleman et al. 1994; Nelson and O'Connor 1964; Richter et al. 1991) have all been used. Depending upon the nature of the material under analysis, compared to XRD, the other techniques may have their advantages. For instance, compared to XRD, NMR and Raman are more appropriate for measurement of CrIs of water-containing samples. Similarly, if a material's composition is such that it contains lignin or hemicelluloses (e.g., wood), Raman spectroscopy provides a more accurate estimation than either XRD or NMR (Agarwal et al. 2013).

In general, limited information is available on how the existence of water in a cellulose sample impacts its XRD profile and therefore, a sample's estimated CrI and L_{200}. A few of the publications that have investigated the role of water focused on the effects of drying and rewetting of wood (Abe and Yamamoto 2005, 2006; Hill et al. 2010; Nishimura et al. 1981; Sugino et al. 2007; Zabler et al. 2010) and dehydration of cotton and bacterial cellulose (Astley et al. 2001; Fang and Catchmark 2014; Fink et al. 1997; Hu and Hsieh 2001). While using XRD (WAXS) in transmission mode, Nishimura et al. (1981) reported that for wood sections the (200) peak shifted to higher 2θ with increasing moisture content and this observation was independent of the crystallite orientation. A similar moisture dependent shift was also observed for ball milled wood powder. Later investigations by other researchers Abe and Yamamoto (2005), Sugino et al. (2007), and Hill et al. (2010) supported such observations of shifts to higher 2θ and d-spacing reduction upon moistening of wood. Wormald et al. (1996), using ss NMR, reported role of moisture in converting disordered cellulose to ordered cellulose. Sugino et al. (2007) also reported hysteresis in moisture adsorption/desorption isotherms in wood and that wood crystallinity changed upon drying and rewetting. On the other hand, other investigators focused on the role of temperature (Atalla and Whitmore 1978) and fibril disorder (Lindner et al. 2014) on XRD estimated CrI. It seems that removal of sample moisture as a disorder causing factor has received only limited attention.

Using XRD, several investigators studied dehydration of bacterial cellulose (Astley et al. 2001; Fang and Catchmark 2014; Fink et al. 1997) and two Groups have focused on dehydration of cotton (Fang and Catchmark 2014; Hu and Hsieh 2001). The conclusion from such investigations was that material dehydration induced structural changes which were either due to a reduction in crystal size or an increase in crystal disorder.

It is well known that cellulose has high affinity for water. Given that cellulose is a polymer of β-D-glucose this is not surprising because there are three hydroxy groups per glucose repeat unit. However, cellulose does not exist in isolated chain form and its aggregated supramolecular state dictates how extensively or nominally it would interact with water. Such attraction for water has been investigated, for instance, by measuring hygroexpansive (morphology and dimensional changes) behavior of pulp fibers (Lee et al. 2012). Likewise, on a macro scale, the effect of

humidity on cellulose materials and their properties are well known. Undoubtedly, in a multi-component material like wood or pulp fibers, some of the observed effect is likely to be caused by non-cellulosic matrix components (e.g., hemicellulose) but the majority of the effect has been attributed to cellulose due to its being the dominant component (at times ≥40%), although the nature of its aggregated state plays an important role. In one instance, how cellulose crystallinity influences the absorbability of water has been investigated (Awa et al. 2014). Another study (Driemeier and Bragatto 2013) reported that cellulose crystalline width plays a role in monolayer hydration of various plant celluloses.

This investigation is a first systematic study of the role of moisture content of cellulose materials on CrI and L_{200}. In addition to the variation of the CrI among the selected materials, the ultrastructure of the aggregated cellulose varied between the materials because the natures of their aggregated states were very different. The CrIs of the materials varied from high (tunicin) to low or non-crystalline (loblolly pine wood). The remaining selected samples, which had intermediate CrIs, consisted of two microcrystalline celluloses (cotton and pulp based), four isolated NaOH treated wood holopulps that were dried differently, a bleached softwood kraft pulp, and a pulp cellulose nanocrystal.

Experimental

Materials

Table 1 lists the materials and their compositions that were used in this study. Tunicate (T, Table 1) was a gift from Dr. Akira Isogai (Tokyo University, Japan). Whatman CC31 powder (MCC1, Table 1) was from Whatman International Ltd., (Maidstone, UK) and Avicel PH-101 (MCC2, Table 1) was from FMC Corporation (Newark, Delaware). BNSWKP (bleached northern softwood kraft pulp, KP, Table 1) was obtained from NIST (Reference materials 8495, National Institute of Standards and Technology, Gaithersburg, MD. Loblolly pine (*Pinus taeda L.*, W, Table 1) 40 mesh was available at the Forest Products Laboratory (FPL). NaOH treated wood holopulp samples (HP1 to HP2od, Table 1) were the same as used previously (Agarwal et al. 2016) and were obtained from hardwood aspen (*Populous tremuloides*) and the softwood red pine (*pinus resinosa*). It's important to note that the wood samples were delignified at room temperature using a procedure similar to that of Atalla et al. (2014) and that subsequently the holopulps were treated by alkali at room temperature (Agarwal et al. 2016). A portion of the samples HP1 and HP2 were vacuum oven dried (110 °C for 24 h) and these were called HP1od (oven dried NaOH treated aspen holopulp) and HP2od (oven dried NaOH treated red pine holopulp). For production of CNCs (cellulose nanocrystals; CNC, Table 1), bleached Kraft pulp was obtained commercially. The method of Reiner and Rudie (2013) was used to produce the CNCs from softwood kraft pulp (SWKP). The sulfur content of the CNCs was 1.1% which was a measure of their surface charge. This method uses 64% sulfuric acid for hydrolyzing the pulp. A similar method was used to produce CNCs from wood and has been reported in detail earlier (Agarwal et al. 2016).

Chemical compositions

Chemical compositions of the samples listed in Table 1 were obtained. The amounts of Klason lignin and carbohydrates were determined using the TAPPI test method (1983) and Davis (1998), respectively. Reproducibility for Klason lignin was 0.4%, and for the carbohydrate analysis, the standard deviation was 1% (Davis 1998).

Drying of sample pellets at room temperature

From each of the materials one 100 mg pellet was prepared using a pellet press. More details can be found elsewhere (Agarwal et al. 2010).

For further drying the pellets under P_2O_5 and sampling purposes, small sampling chambers were prepared by sealing nylon washers (16 mm O.D., 11 mm I.D.) onto the centers of cleaned microscope slides with a silicone-based sealant. Care was taken to keep the sealant clear of the center hole and without gaps as seen from the back side. The sealant was left to cure.

A 9 mm diameter sample pellet was placed inside the washer and the height of the pellet was less than the top rim of the washer. A thin layer of high vacuum grease was then applied to the top rim of the washer. Each of the slide assemblies was placed in a desiccator

Table 1 Materials used and their compositions

Sample	Description	Composition[a], %						
		KL	Ara	Gal	Glu	Xyl	Man	Hemi
T	Tunicate	1.5	ND	ND	94.6	ND	ND	ND
MCC1	Whatman CC31	3.1	ND	ND	92.2	0.1	ND	ND
MCC2	Avicel PH 101	0.4	ND	ND	93.4	0.8	1.7	2.9
CNC	BSWKP-CNCs[b]	0.3	ND	ND	85.4	3.1	ND	3.1
KP	BNSWKP[c]	0.5	0.3	ND	81.3	7.5	5.2	14.0
HP1	NaOH treated aspen holopulp	1.6	0.1	0.3	73.0	6.6	3.5	10.5
HP1od	Oven dried NaOH treated aspen holopulp	1.6	0.1	0.3	73.0	6.6	3.5	10.5
HP2	NaOH treated red pine holopulp	0.8	0.6	0.9	69.1	3.2	14.4	19.1
HP2od	Oven dried NaOH treated red pine holopulp	0.8	0.6	0.9	69.1	3.2	14.4	19.1
W	Loblolly pine, 40 mesh	30.7	1.5	2.4	41.3	6.2	9.7	19.8

[a] KL Klason lignin, Ara arabinan, Gal galactan, Glu glucan, Xyl xylan, Man mannan, Hemi hemicellulose (content of hemicellulose was obtained by adding all the non-glucose sugars)

[b] Bleached softwood kraft pulp cellulose nanocrystals

[c] Bleached northern softwood kraft pulp

over Drierite along with a watch glass containing anhydrous P_2O_5 and a rack of thin, square cover slips. The samples were kept drying for 2 weeks and initially, the P_2O_5 was changed daily and then periodically on as needed basis.

The desiccator was placed in a glove bag along with a dish of Drierite desiccant. The bag was evacuated and then purged with dry nitrogen gas 5 times and then filled to a workable level with dry nitrogen and left over the weekend.

The desiccator was then opened in the glove bag and using a forceps a cover slip was dropped onto the greased washer and pressed to seal. Once all of the samples were sealed the slides were removed from the glove-bag and the cover slips gently taped, each side to the glass slide. The samples were kept sealed in an air-tight box until analyzed.

X-ray measurements

Wide-angle X-ray scattering (WAXS) profiles were recorded using a Bruker D8 Discover diffractometer at the Materials Research Science and Engineering Center, University of Wisconsin, Madison. The diffractometer was equipped with a VÅNTEC-500 detector and the samples were analyzed in the reflection mode. The incident X-ray radiation was monochromatic CuKα ($\lambda = 1.5418$ Å) point source. An X-ray diffractometer beam aperture of 0.5 mm was used. Except where stated otherwise, pellets were sampled on both sides and average values of XRD parameters along with corresponding SD data are reported. The reported SD represents spread between repeated measurements.

For WAXS, to minimize exposure to ambient air, each P_2O_5 dried sample pellet was kept sealed until just before sampling when a side tape was cut and the cover slip pulled back. Diffractograms were recorded on both sides of all the dry pellets. Subsequently, 5 μL water was added to the center of the pellet surface using a syringe. Once the water disappeared from the surface and was absorbed by the pellet a diffractogram was obtained. Then, the pellet was overturned and the other side was analyzed. Additional water was not applied to the other side. Upon adding the small amount of water, only loblolly pine pellet (W, Table 1) did not retain its shape and could not be turned over. Therefore, in this case, only a single XRD was obtained after water was added.

To evaluate the effect of drying, post moistening, another set of XRD experiments was carried out. Pellets from a subset of samples (T, MCC2, CNC, HP1, HP2, W; Table 1) were analyzed by XRD. Initially, these samples were dried under ambient

conditions (temperature 25 °C; RH 15%) and pressed into pellets. Subsequently, XRDs of the sample pellets were obtained in the following order—(a) in dried state, (b) in moist state after 5 μL added water was absorbed by the pellet, (c) in partly dried state—at 15 min interval from step (b), and lastly, (c) after further drying, at 70 min interval from step (b). In this XRD investigation, the pellets were analyzed only on one side.

FWHM and peak position for the (200) reflection were determined from the diffractograms of the samples after a Gaussian profile function was fitted between 2θ of 18° and 29°. This was done to smooth out the effect of noise in the diffractogram. To minimize the effect of noise, the Gaussian function fitted between 2θ 18° and 29° was only applied for determining FWHM and the (200) position, but not for signal intensity. This was done not to artificially deconvolute the (200) diffraction peak profile because there are issues with not only deconvolution approaches but also the assumptions that have to do with what are the contributors to a sample's diffractogram. Segal-WAXS CrI was calculated using the Segal method, Eq. 1 (Segal et al. 1959) with the amorphous content measured at ~18° and crystalline amount at ~22.5° after a background was subtracted from each of the diffractograms. The diffractograms were background corrected using "rubber band correction" (a polynomial correction, in OPUS 7.2, Bruker Inc.). This method uses—figuratively speaking—a rubber band which is stretched between the spectrum endpoints. The rubber band follows the diffractogram minima.

$$\mathrm{CrI} = (\mathrm{I}_{22.5} - \mathrm{I}_{18}) \times 100/\mathrm{I}_{22.5} \quad (1)$$

In most cases, the crystallites of cellulose making up the materials are small and therefore, broadened X-ray diffractograms were obtained. This broadening is inversely proportional to the size of the crystallite. The Scherrer equation, Eq. 2 (Scherrer 1918; Langford and Wilson 1978) was used to measure the crystallite size, L_{200}. Here the shape factor (usually called K, depends upon the shape of the crystallites) is taken as 0.9.

$$\mathrm{L} = (0.9 \times \lambda/\beta \times \mathrm{Cos}\theta) \quad (2)$$

To calculate L_{200} in nanometers, λ the X-ray wavelength is taken as 0.15418 nm, β is the peak width of the (200) profile at half maximum (FWHM) in radians. θ is the half of the (200) Bragg diffraction peak position (2θ max position) in radians. However, French and Santiago Cintrón (2013) showed that measured FWHM values increased because of increasing FWHM values. Therefore, experimentally measured values did not truly reflect actual crystallite sizes due to increased peak overlap.

Statistical test

The nonparametric "sign test" (Hollander et al. 2014) was performed for all four response variables (CrI, 2θ max position, FWHM, and L_{200}). However, it must to be noted that L_{200} is a function of 2θ and FWHM and therefore, it is not an independent variable. The sign test is perhaps the simplest of the nonparametric statistical tests. We describe it below. The R software environment (R Core Team 2013; The R Project for Statistical Computing) was used to do the sign test.

There were 10 materials. A pellet was prepared for each material, and the pellet was measured in both the dry and moist states. Because of random variation in response measurement, if there were no systematic difference between the dry and moist states, for a given material the probability that the dry measurement (in the present context, any of the four variables CrI, 2θ max, FWHM, or L_{200}) would be less than the moist measurement would be 1/2. The probability that the dry measurement would be less than the moist measurement for all 10 materials would be $(1/2)^{10} = 1/1024 = 0.00098$ (the probability that a flip of a fair coin comes up heads in 10 consecutive flips). Similarly, the probability that the dry measurement would be greater than the moist measurement for all 10 materials would be 0.00098. Thus, if there were no systematic difference between the dry and moist measurements, the probability that the ordering of the dry and moist observations would be the same for all 10 materials would be $2/1024 = 0.002$. Thus, if for one of the four response variables, we see the same ordering for all 10 materials (either all the dry measurements are greater than the moist measurements or all the dry measurements are lower than the moist measurements), we can reject the hypothesis of no difference between the dry and moist measurements at a 0.002 significance level. That is, either there is a systematic difference between the dry and moist measurements or we have seen a result that occurs very rarely.

Results and discussion

Diffractograms of pellets of the samples listed in Table 1 were obtained in dry (P_2O_5 dried) and moist states. Diffractograms of a few selected samples (T, MCC2, HP2od, W) are shown in Fig. 1a–d and for others in Fig SI1 (in the SI section). Except for Fig. 1d (representing sample W), all other sub-Figs in Fig. 1 and Fig. SI1 consist of four diffractograms—two each obtained in dry and moist states. For sample W (Fig. 1d), although two X-ray diffractograms could be obtained in the dry state, only one could be obtained in the moist state after 5 µL water was added to the surface of the pellet. The pellet integrity was lost and it could not be turned over.

From the diffractograms, obtained in dry and moist states, various sample parameters (CrI, 2θ max, FWHM, and L_{200}) were determined and are listed in Table 2. The impact of moisture on the sample diffractograms can be noted from Figs. 1 and SI1 and on the sample parameters from Figs. 2, 3, 4, 5 and 6 where the differences between dry and moist states are reported. In Table 2, average data with standard deviation (SD) for CrI, 2θ max position, FWHM, and L_{200} are compared. For sample W in the moist state, no SD is given because only one side of the pellet could be sampled. Water addition to the samples causes significantly different effects on the samples. In the following, each of the four XRD measurements is discussed individually.

CrI change

Segal CrIs are reported in Table 2. For most samples, the SD values are reasonable and in the range previously reported by Agarwal et al. (2014). In that investigation, compared to the milled wood samples the authors reported higher SDs for rectangular wood blocks. It is likely that the higher SDs were caused by the orientation differences of the cellulose fibers in the blocks. Among the samples in Table 2 that showed high SD, most were associated with the moistened pellets where the diffractograms obtained from the two sides were quite different (e.g., Fig. 1c).

Based on the data in Table 2, differences between the moist and dry sample Segal CrIs are plotted in Fig. 2. Of the ten samples analyzed, the most to least CrI increase order (% value in parentheses) was as follows—HP2od (36.7) > W (32.9) > HP1od (29.0) > KP (25) > HP2(18.1) > CNC (10.6) > HP1 (9.1) > MCC2 (8.9) > MCC1 (4.0) > T (0.2). Upon sample moistening (5 µL water addition), the CrI increased by 37% for HP2od and 33% for W whereas almost no change occurred for T and very little (4%) for MCC1, the latter two being highly crystalline materials (dry CrIs 97 and 94%, respectively,

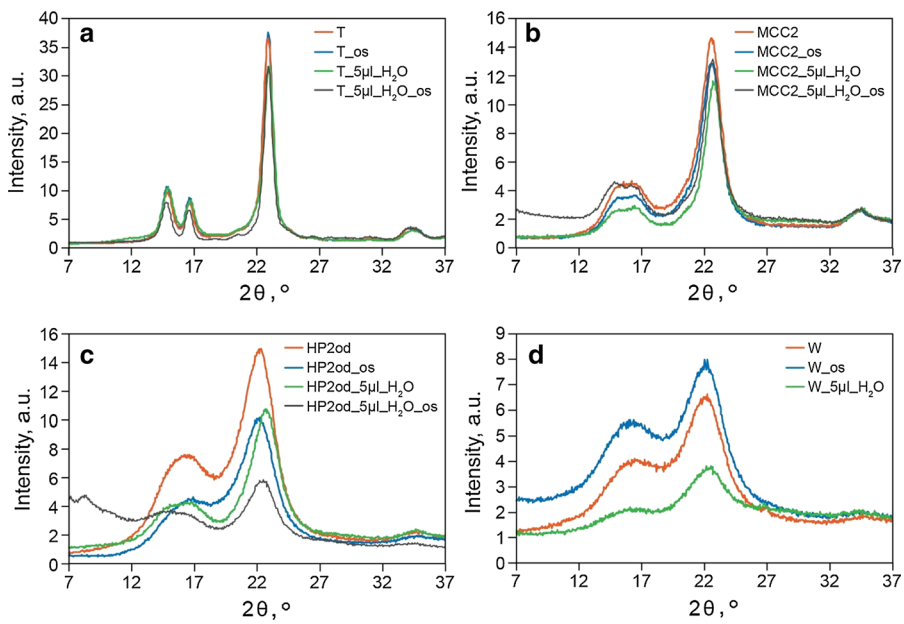

Fig. 1 X-ray diffractograms of P_2O_5 dried and moistened sample pellets **a** T, **b** MCC2, **c** HP2od, **d** W; os means other side of the pellet

Table 2 XRD parameters for P_2O_5 dried and moist pellets

Sample	% CrI, Segal		(200) Peak position, 2θ		(200) FWHM		Crystallite size, L_{200}	
	Dry	Moist	Dry	Moist	Dry	Moist	Dry	Moist
T	97.2 ± 0.09	97.4 ± 2.4	22.9 ± 0.01	23.0 ± 0.03	0.89 ± 0.03	0.85 ± 0.09	9.1 ± 0.26	9.55 ± 0.99
MCC1	94.3 ± 0.57	98.0 ± 0.50	22.7 ± 0.03	22.8 ± 0.07	1.28 ± 0.00	1.09 ± 0.01	6.3 ± 0.01	7.46 ± 0.04
MCC2	88.4 ± 1.81	96.3 ± 1.0	22.5 ± 0.00	22.7 ± 0.08	1.87 ± 0.05	1.56 ± 0.00	4.3 ± 0.11	5.20 ± 0.01
CNC	84.4 ± 0.11	93.4 ± 3.2	22.6 ± 0.01	22.7 ± 0.17	2.25 ± 0.01	1.82 ± 0.18	3.6 ± 0.01	4.47 ± 0.32
KP	74.7 ± 0.51	93.0 ± 0.30	22.3 ± 0.01	22.6 ± 0.06	2.21 ± 0.00	1.79 ± 0.08	3.7 ± 0.01	4.54 ± 0.20
HP1	83.4 ± 4.77	91.0 ± 4.3	22.4 ± 0.09	22.6 ± 0.05	2.59 ± 0.14	2.31 ± 0.13	3.1 ± 0.17	3.52 ± 0.20
HP1od	71.5 ± 0.16	92.3 ± 0.10	22.0 ± 0.02	22.5 ± 0.03	3.18 ± 0.06	2.27 ± 0.11	2.5 ± 0.05	3.57 ± 0.18
HP2	76.2 ± 1.27	89.9 ± 1.8	22.2 ± 0.01	22.4 ± 0.19	3.05 ± 0.07	2.60 ± 0.26	2.7 ± 0.06	3.13 ± 0.32
HP2od	65.7 ± 0.17	89.8 ± 7.4	21.9 ± 0.01	22.5 ± 0.25	3.77 ± 0.01	2.74 ± 0.13	2.1 ± 0.01	2.97 ± 0.20
W	55.5 ± 1.72	73.7 ± NA	21.8 ± 0.06	22.3 ± NA	4.49 ± 0.20	3.03 ± NA	1.8 ± 0.08	2.70 ± NA

After adding 5 µL water

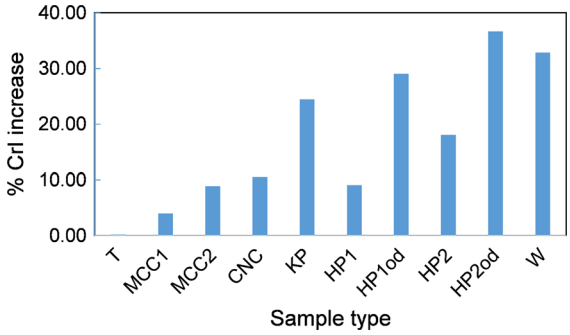

Fig. 2 Percentage of increase in CrI upon 5 µL water addition

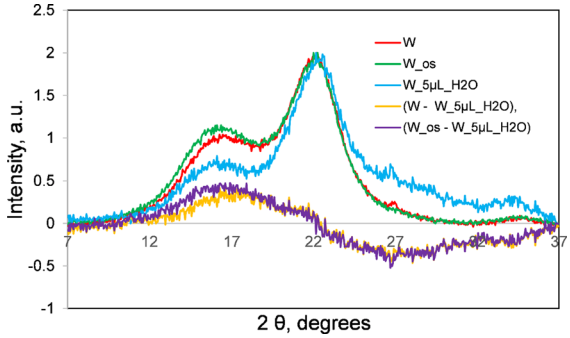

Fig. 3 2θ max position for (200) reflection, W in dried state (W) and after 5 µL water addition (W_5 µL_H_2O); os means other side of the pellet. Subtracted spectra (W–W_5 µL_H_2O), and (W_os–W_5 µL_H_2O) are shown as well

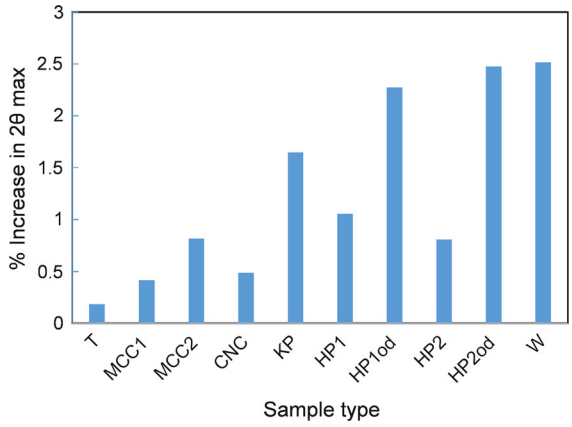

Fig. 4 Percentage of increase in 2θ max position for (200) reflection

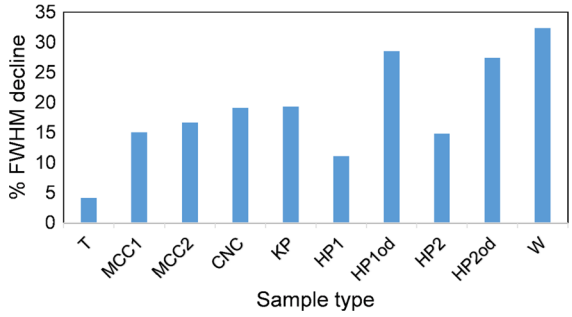

Fig. 5 Percentage of decline in FWHM after 5 µL water addition

Table 2). In contrast, in the case of W which was P_2O_5 dried at 25 °C, cellulose molecules are expected to be present in a state that is only slightly modified from their existence in the native state (Agarwal et al. 2016). The authors reported that in the native state ~50% of wood cellulose is accessible by water.

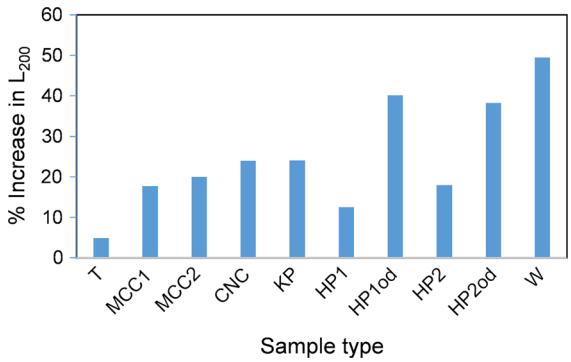

Fig. 6 Percentage of increase in L_{200} after 5 μL water addition

Compared to the dried state, upon addition of water, significant ordering of the cellulose chains seems to take place. Additional evidence for this came from the FWHM data (Table 2, more below), which showed a significant narrowing of the (200) peak. Previously, XRD FWHM for (200) and water accessibility of wood cellulose have been found to be positively correlated (Agarwal et al. 2016). In that paper, the authors suggested that the (200) FWHM can be taken as a measure of existing disorder in cellulose.

On the other hand, due to T's high crystalline nature, upon water addition, the sample underwent no such reordering of the interior cellulose chains (CrI changes of 0.2%, Fig. 2). Only surface chains are available for interaction with water. But it appears that such an interaction was not enough to bring about a meaningful change in the CrI. This explains why the CrI for the sample remained unchanged. It is important to note that the contribution of water's diffractogram to the sample diffractograms can be ruled out based on the fact that (a) the moistened T sample did not show any significant change in its diffractogram (Fig. 1a, T vs. T–5 μL–H_2O) and (b) water's diffractogram (Fig. SI2) indicated that most contribution occurs at $2\theta > 27°$. The latter is supported by the literature reported water peak at 28.5° (2θ) in XRD (Fang and Catchmark 2014). Furthermore, because sample XRDs were obtained after water was completely absorbed by the samples, it's likely to be only present in a molecularly dispersed state and not exist as a separate phase. In any case, in the XRDs of the samples, no peak due to water at 28.5° (2θ) was detected.

Moistening of the samples of kraft pulp (KP), three of the NaOH treated holocellulose samples (HP2, HP1od, and HP2od), and CNC showed significant CrI increases (37–9%; Fig. 2). In contrast, microcrystalline celluloses from cotton (MCC1) showed only a small increase (4%). Additionally, compared to 25° C dried samples HP1 and HP2, the corresponding oven dried equivalents HP1od and HP2od showed higher CrI change (Fig. 2). The latter suggested that oven drying induced more disorder between cellulose chains (the CrIs of the oven dried samples were lower compared to their 25 °C dried equivalents, Table 2) and this thermally induced disorder seem to have been quenched to a considerable degree upon water addition as evidenced by the resultant CrI increases for the moist samples (Table 2).

In addition to wood (W), three pulp samples (KP, HP1od, HP2od) showed high % CrI increases (Fig. 2). To explain the differences in the crystallinity behaviors between KP, HP1od, and HP2od their compositional differences were considered. The compositions of various samples are reported in Table 1. The glucan content for the samples KP, HP1od, and HP2od are 81.3, 73, and 69.1%, respectively. Moreover, compared to HP1od, both KP and HP2od have slightly higher amounts of hemicelluloses—10.5% in HP1od versus 14 and 19.1% in KP and HP2od, respectively (Table 1). However, in these pulps, the order of CrI increases does not correlate with the amount of hemicellulose present. Also, the CrI increase in HP2 is lower compared to that of KP whereas the former has higher amount of hemicellulose (Table 1). Consequently, in the case of HPod1 and HPod2, there must be a contribution due to oven drying. Therefore, hemicellulose difference is not likely to be the reason why compared to KP, HP1od and HP2od showed higher CrI increases. Moreover, simply having a higher cellulose or glucan content does not seem to be the reason either because compared to HP2, HP1 had more cellulose but showed lower increase upon water addition (Fig. 2). The explanation for the latter observation may have to do with the difference in the hemicellulose content of the two samples—HP2 had 9% more hemicellulose (Table 1). Therefore, the only explanation seems to lie in the differences between the ultrastructures of the celluloses between the samples (KP, HP1, HP2, HP1od, HP2od). The cellulose structures and hence their susceptibility to water is likely to be different due to the fact that these samples were produced with two different processes. Whereas KP is a kraft pulp sample which was treated at high temperature (170 °C) with alkali, both HP1 and

HP2 underwent mild treatments (acid chlorite delignification and mild NaOH treatments both at 25 °C—Agarwal et al. 2016).

2θ max position change

Upon sample moistening (5 μL water addition), in all cases, the (200) 2θ max position shifted slightly to higher values (Table 2). For the wood sample (W), the shift can be clearly seen in Fig. 3 where the diffractograms for dry and moist states are plotted after background subtraction and (200) peak normalization. Figure 3 also shows how water addition causes the X-ray scattering to decline in 12°–22° (2θ) and to increase in 22°–37° (2θ). Such changes are likely to be associated with the alterations in the organization of the scattering components because sample composition remains same. As shown in Fig. 4, between the samples, the % increase in 2θ max position varied. The shift was hardly detectable for T (0.2% increase, Fig. 4; Table 2), whereas was 12.5 times higher at 2.5% for W (Fig. 4; Table 2). In case of woods, such a shift has been previously reported (Abe and Yamamoto 2005, 2006; Hill et al. 2010; Nishimura et al. 1981; Sugino et al. 2007; Zabler et al. 2010). The 2θ max position was also shifted to higher values in most of the non-wood samples (Fig. 4; Table 2). The compositional data in Table 1 and plots in Fig. 4 suggest that % increases in 2θ max position are not due to lignin. Comparing the oven (110 °C) versus room temperature (25 °C) dried samples (HP1od and HP2od vs. HP1 and HP2), the (200) peak of the former samples shifted by larger amounts (Fig. 4). This is likely to be due to the presence of more disordered cellulose and hemicelluloses in the oven dried materials compared to their room temperature equivalents. Because KP's 2θ max position shift was lower compared to that of HP1od and HP2od samples, it suggested that compared to KP more disordered cellulose (and hemicellulose) exists in the holopulp samples that were heated to 110 °C (HP1od and HP2od). In particular, in both these oven dried holopulp samples, cellulose (and hemicellulose) has the characteristic of becoming more ordered upon water addition.

It is interesting that, upon sample moistening, compared to the highly crystalline T, CNC showed greater shift in (200) 2θ max position. This is likely to be a consequence of the fact that compared to T, CNC has a smaller L_{200} (Table 2) and therefore, the latter sample has higher surface area. This means that CNC has more cellulose chains on the crystallite surfaces which in turn, upon moistening, are capable of reorienting by interacting with the molecules of added water. The other change could be straightening (by reorientation) of the chain-sections at the ends of the CNCs. The net effect of the two processes could be a reduction in inter-planer distance.

FWHM and L_{200} change

Except for T which showed hardly any decline in (200) FWHM (4%, Table 2), all other moist cellulose materials showed a decline in FWHM (Fig. 5; Table 2). The highest reduction in FWHM was observed for the wood sample (W, Fig. 5). The FWHM decline in T was very small, 4% is within experimental error (Table 2). In all cases, the narrowing of the (200) peak in the diffractograms seems to be associated with the reorganization of the cellulose chains although in samples that contained hemicellulose its role cannot be ruled out. However, the extent of the cellulose reorganization varies between the samples and in some cases (e.g., W) it is expected to take place in the interior of the sample due to the fact that the interior cellulose chains are water accessible (Agarwal et al. 2016). In the case of samples other than W, "hypothesis of drying stresses" can also be invoked because these samples are known to be partially crystalline, although for cellulose materials, the hypothesis of drying stresses has never been proven. Nevertheless, even assuming no access of water to polymers located in the interior of the crystalline fibril, net observed changes would be a result of two distinct contributions—(a) the drying stresses part and (b) the water-polymer interaction induced changes part (occurring in the non-crystalline regions of the fibrils). Noteworthy in this regard is the special status of sample W where the contribution (a) does not exist. In other samples contribution (a) (and therefore b) will vary depending upon the level of crystallinity of the sample.

The decline in FWHM of the other samples was directly responsible for the increased L_{200} (Eq. 2; Table 2). The % increase in the L_{200} is plotted in Fig. 6. The relationship between FWHM and L_{200} is clear from the Scherrer equation (Eq. 2). The order in which crystallite size increased in the moistened

samples was as follows (% values in parentheses)—W (49.5) > HP1od (40.2) > HP2od (38.2) > CNC (24.1) = KP (24.1) > MCC2 (20) > HP2 (18) ≥ MCC1 (17.8) > HP1 (12.5) > T (4.9). Clearly, W showed the most increase in the crystallite size. It is important to note that the L_{200} values are based on the observed (200) FWHMs and contributions of lignin and hemicelluloses to the W's diffractogram, if any, were still present. Because, in XRD, both lignin and hemicelluloses contribute in some of the same 2θ regions as the cellulose peak (200) (Agarwal et al. 2013), theoretically, one can make the argument that at least in the case of W the diffractogram needs to be corrected prior to calculating the L_{200}. However, given that such a correction is not straightforward and complexities arise that are not addressable in a satisfactory way, such a need cannot be justly fulfilled. Specifically, issues that have to do with the contributions to the broadening of the wood diffractogram peak and the extent to which disorganized cellulose itself is responsible for it. Moreover, unanswered remains the question about the XRD contributions of lignin and hemicelluloses when they exist as a separate phase versus in molecularly distributed form (as they do in wood). Furthermore, it has become increasingly clear that various treatments (physical, chemical, and thermal) of wood modify the native state structure of cellulose to various degrees (Agarwal 2016; Agarwal et al. 2016; Atalla et al. 2014; Langan et al. 2014; Nishiyama et al. 2014; Toba et al. 2013). Upon chemical treatment, the (200) peak of the treated wood narrows, but whether this is due to removal of non-cellulose component(s) or alterations of cellulose structure is unknown. And, in case both these factors play a role then to what degree is not easily discernable. Therefore, in the case of W and the other samples, the authors have decided not to make a correction prior to estimating L_{200}. Besides, in this investigation, the objective is to determine how moistening impacts these XRD parameters for the whole sample.

Sign test

Based on data in Table 2, for all four response variables (CrI, 2θ max position, FWHM, and L_{200}), either the dry measurement was less than the corresponding moist measurement for all 10 materials, or the dry measurement was greater than the corresponding moist measurement for all 10 materials. Thus, the p values for all four comparisons were 0.002. If we want to take into account the fact that we are making four comparisons, then a Bonferroni multiple comparison approach (Miller 1981) would still yield 0.008 p values. Therefore, the null hypothesis that there are no differences between the response variables of moist and dried samples is rejected at this level.

Correlations of the changes with sample CrIs

The % changes in each of the four parameters (CrI, 2θ max position, FWHM, and L_{200}) were correlated with dry sample CrIs to find out if these variables depended upon Segal crystallinities of the samples (Fig. 7). All the correlations were positive (Fig. 7, R^2 between 0.87 and 0.76) which meant that, upon moistening, the % increases in CrI (Fig. 7a), 2θ max position (Fig. 7b), and L_{200} (Fig. 7d) declined with increase in the sample CrIs. In contrast, the % reduction in FWHM declined with increase in sample CrI (Fig. 7c). The factor that fluctuated in tandem most with the sample CrIs was % increase in CrI (Fig. 7a, $R^2 = 0.87$).

Longer duration drying post moistening

To assess the effect of longer duration drying post moistening, pellets of selected samples (Table 3) that were initially dried under ambient conditions were used. As before, diffractograms were obtained from dried and moist (5 μL H_2O) pellets, but only from one side. The pellets were not turned over. Additionally, pellet diffractograms were obtained after 15 and 70 min of the pellet moistening step. From the diffractograms, CrI and FWHM data were obtained (Table 3). In Fig. 8, the effect of longer duration drying on the CrIs is shown and it can be noted that in cases where the CrI had increased upon moistening, it declined upon drying of the samples. Based on the comparison of the CrIs that were obtained initially and after 70 min of pellet drying (Table 3; Fig. 8), for all samples, the two values were similar.

FWHM data (Table 3) are plotted in Fig. 9 wherein the effect of longer duration drying can be observed. As expected (see above), upon water addition, initially the FWHM declined in most cases but the peak width increased upon drying (Fig. 9; Table 3). And at 70 min point, for each sample, the FWHM was closer

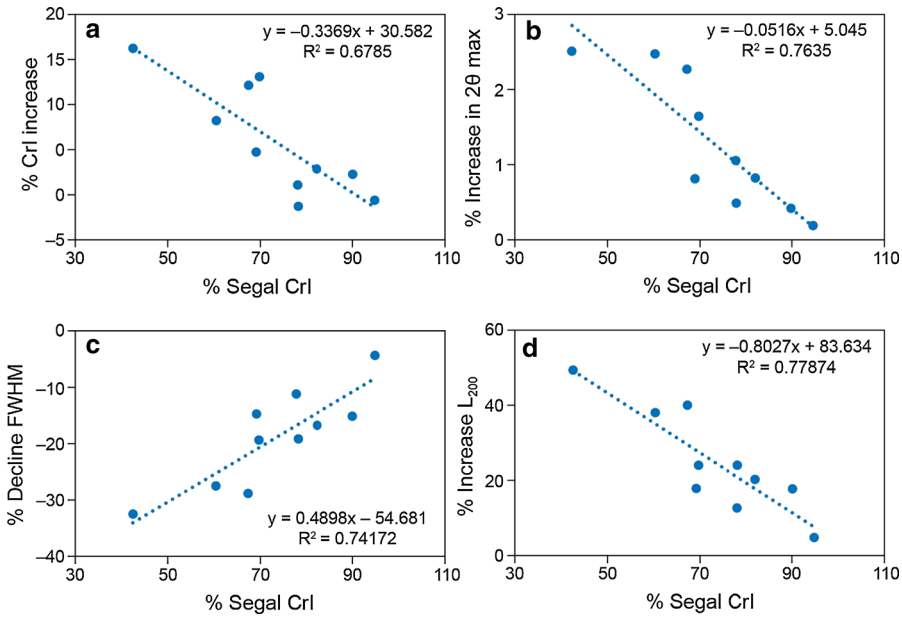

Fig. 7 Correlations of various XRD parameters with sample dry state Segal CrI; **a** % increase in CrI, **b** % increase in 2θ max position, **c** % decline in (200) FWHM, **d** % increase in L_{200}

Table 3 CrI and FWHM changes upon 15 and 70 min drying post moistening of 25 °C dried (ambient) pellets

Sample	% CrI, Segal				(200) FWHM			
	Dry	Moist[a]	15 min later	70 min later	Dry	Moist	15 min later	70 min later
T	96.4	100.1	98.0	97.2	0.95	0.80	0.94	0.88
MCC2	87.1	98.0	89.8	88.8	1.99	1.56	1.86	1.93
CNC	82.9	94.8	86.7	84.8	2.43	1.88	2.30	2.33
HP1	76.5	94.0	88.2	81.1	2.95	2.25	2.53	2.68
HP2	74.4	90.2	82.9	79.3	3.13	2.55	2.80	2.85
W	62.9	77.8	73.6	67.0	4.00	3.20	3.20	3.60

[a] After adding 5 µL water

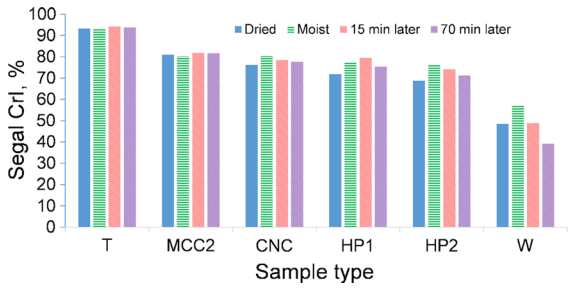

Fig. 8 Segal CrIs in dried (ambient) state, upon 5 µL water addition, and after 15 and 70 min drying

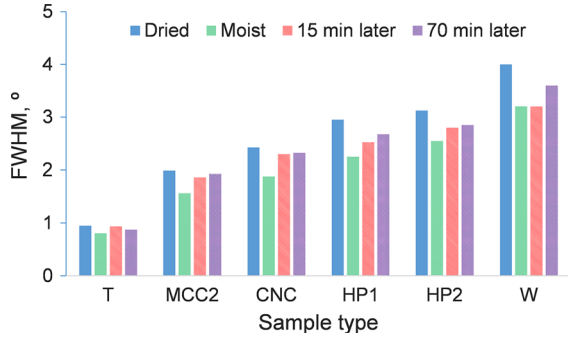

Fig. 9 (200) FWHM in dried state, upon 5 µL water addition, and after 15 and 70 min drying

in value to that obtained in the initial dried state. However, because in all cases the 70 min values were slightly lower than those obtained initially (Table 3), it's likely that even after 70 min the pellets were not completely dry.

Conclusions

For various cellulose samples, the effect of moisture change upon diffractogram derived parameters was investigated. It was found that CrI, (200) 2θ max position, FWHM, and L_{200} were all affected to varying degrees depending upon the nature of the sample. In general, higher levels of change were associated with samples that had lower CrIs. The two extreme examples were tunicin and loblolly pine wood where, for most variables, the least and greatest changes were detected, respectively. These conclusions were supported by the statistical analysis that was based on the sign test. When the moistened samples were dried for longer duration, it was observed that these changes were reversible to a degree. The implication for practical work is that when XRD is used to compare sample characteristics, the analysis needs to take place under similar moistness levels. This means that the samples need to be conditioned and tested at similar humidity levels. This is particularly important when samples are being compared that were analyzed in different seasons at varying relative humidity. Significant differences exist between seasonal humidity levels and therefore, sample moistness levels.

Acknowledgments The authors thank Dr. Akira Isogai (Tokyo University) for providing Tunicate cellulose. The authors acknowledge Fred Matt of the FPL Analytical Chemistry and Microscopy Laboratory Unit for carrying out the composition analyses of the samples. The authors gratefully acknowledge use of X-ray facilities and instrumentation supported by NSF through the University of Wisconsin Materials Research Science and Engineering Center (DMR-1121288).

References

Abe K, Yamamoto H (2005) Mechanical interaction between cellulose microfibril and matrix substance in wood cell wall determination by X-ray diffraction. J Wood Sci 51:334–338

Abe K, Yamamoto H (2006) Change in mechanical interaction between cellulose microfibril and matrix substance in wood cell wall induced by hygrothermal treatment. J Wood Sci 52:107–110

Agarwal UP (2016) Evolution of wood-cellulose native structure upon thermal and hydrothermal Treatments. CELL Division Abstract # 202, ACS, 251st meeting, San Diego

Agarwal UP, Reiner RS, Ralph SA (2010) Cellulose I crystallinity determination using FT–Raman spectroscopy: univariate and multivariate methods. Cellulose 17:721–733

Agarwal UP, Reiner RS, Ralph SA (2013) Estimation of cellulose crystallinity of lignocelluloses using near-IR FT–Raman spectroscopy and comparison of the Raman and Segal-WAXS methods. J Agric Food Chem 61:103–113

Agarwal UP, Ralph SA, Reiner RS, Moore RK, Baez C (2014) Impacts of fiber orientation and milling on observed crystallinity in jack pine. Wood Sci Technol 48:213–1227

Agarwal UP, Ralph SA, Reiner RS, Baez C (2016) Probing crystallinity of never-dried wood cellulose with Raman spectroscopy. Cellulose 23:125–144

Ahvenainen P, Kontro I, Svedstrom K (2016) Comparison of sample crystallinity determination methods by X-ray diffraction for challenging cellulose I materials. Cellulose 23:1073–1086

Armstrong RC, Wolfram C, de Jong KP, Gross R, Lewis NS, Boardman B, Ragauskas AJ, Ehrhardt-Martinez K, Crabtree G, Ramana MV (2016) The frontiers of energy. Nat Energy 1:15020

Astley OM, Chanliaud E, Donald AM, Gidley MJ (2001) Structure of acetobacter cellulose composites in the hydrated state. Int J Biol Macromol 29:193–202

Atalla RH, Whitmore RE (1978) The influence of elevated temperatures on structures in the isolation of native cellulose. J Poly Sci Poly Lett Ed 16:601405

Atalla RS, Crowley MF, Himmel ME, Atalla RH (2014) Irreversible transformations of native celluloses, upon exposure to elevated temperatures. Carbohydr Poly 100:2–8

Awa K, Shinzawa H, Ozaki Y (2014) An effect of cellulose crystallinity on the moisture absorbability of a pharmaceutical tablet studied by near-infrared spectroscopy. Appl Spectrosc 68:625–632

Barnette AL, Lee C, Bradley LC, Schreiner EP, Park YB, Shin H, Cosgrove DJ, Park S, Kim SH (2012) Quantification of crystalline cellulose in lignocellulosic biomass using sum frequency generation (SFG) vibration spectroscopy and comparison with other analytical methods. Carbohydr Poly 89:802–809

Bertran MS, Dale BE (1986) Determination of cellulose accessibility by differential scanning calorimetry. J Appl Poly Sci 32:4241–4253

Davis MW (1998) A rapid method for compositional carbohydrate analysis of lignocellulosics by high pH anion-exchange chromatography with pulse amperometric detection (HPAE/PAD). J Wood Chem Technol 18:235–252

Driemeier C, Bragatto J (2013) Crystallite width determines monolayer Hydration across a wide spectrum of celluloses isolated from plants. J Phys Chem B 117:415–421

Eichhorn SJ (2011) Cellulose nanowhiskers: promising materials for advanced applications. Soft Matter 7:303–315

Fang L, Catchmark JM (2014) Structure characterization of native cellulose during dehydration and rehydration. Cellulose 21:3951–3963

Favier V, Chanzy H, Cavaille JY (1995) Polymer nanocomposites reinforced by cellulose whiskers. Macromolecules 28:6365–6367

Fink HP, Purz HJ, Bohn A, Kunze J (1997) Investigation of the supramolecular structure of never dried bacterial cellulose. J Macromol Symp 120:207–217

French AD, Santiago Cintrón M (2013) Cellulose polymorphy, crystallite size, and the Segal crystallinity index. Cellulose 20:583–588

Hill SJ, Kirby NM, Mudie ST, Hawley AM, Ingham B, Franich RA, Newman RH (2010) Effect of drying and rewetting of wood on cellulose molecular packing. Holzforschung 64:421–427

Hollander M, Wolfe DA, Chicken E (2014) Nonparametric statistical methods, 3rd edn. Wiley, Hoboken

Hu X-P, Hsieh Y-L (2001) Effects of dehydration on the crystalline structure and strength of developing cotton fibers. Text Res J 71:231–239

Hulleman SHD, Van Hazendonk JM, Van Dam JEG (1994) Determination of crystallinity in native cellulose from higher plants with diffuse reflectance Fourier transform infrared spectroscopy. Carbohydr Res 261:163–172

Isogai A (2013) Wood nanocelluloses: fundamentals and applications as new bio-based nanomaterials. J Wood Sci 59:449–459

Klemm D, Kramer F, Moritz S, Lindstrom T, Ankerfors M, Gray D, Dorris A (2011) Nanocelluloses: a new family of nature-based materials. Angew Chem Int Ed 50:5438–5466

Langan P, Petridis L, O'Neill HM, Pingali SV, Foston M, Nishiyama Y, Schulz R, Lindner B, Hanson BL, Harton S, Heller WT, Urban W, Evans B, Gnanakaran S, Ragauskas AJ, Smith JC, Davison BH (2014) Common processes drive the thermochemical pretreatment of lignocellulosic biomass. Green Chem 16:63–67

Langford J, Wilson A (1978) Scherrer after sixty years: a survey and some new results in the determination of crystallite size. J Appl Crystallogr 11:102–113

Larsson PT, Hult E-L, Wickholm K, Pettersson E, Iversen T (1999) ^{13}C-NMR spectroscopy applied to structure and interaction studies on cellulose I. Solid State Nucl Magn Reson 15:31–40

Lee JM, Pawlak JJ, Heitmann JA (2012) Dimensional and hygroexpansive behaviors of cellulose microfibrils (MFs) from kraft pulp-based fibers as a function of relative humidity. Holzforschung 66:1001–1008

Lindner B, Petridis L, Langan P, Smith JC (2014) Determination of cellulose crystallinity from powder diffraction diagrams. Biopoly 103:67–73

Miller RG Jr (1981) Simultaneous statistical inference. Springer, New York

Moon RJ, Martini A, Nairn J, Simonsen J, Youngblood J (2011) Cellulose nanomaterials review: structure, properties and nanocomposites. Chem Soc Rev 40:3941–3994

Nelson ML, O'Connor RT (1964) Relation of certain infrared bands to cellulose crystallinity and crystal lattice type. Part I. Spectra of lattice types I, II, III and of amorphous cellulose. J Appl Poly Sci 8:1311–1324

Newman RH (1999) Estimation of the lateral dimensions of cellulose crystallites using ^{13}C NMR signal strengths. Solid State Nucl Magn Reson 15:21–29

Nishimura H, Okano T, Asano I (1981) Fine structure of wood cell walls. I. Structural features of noncrystalline substances in wood cell walls. Mokuzai Gakkaishi 27:611–617

Nishiyama Y, Langan P, Chanzy H (2002) Crystal structure and hydrogen-bonding system in cellulose Iα from synchrotron X-ray and neutron fiber diffraction. J Am Chem Soc 124:9074–9082

Nishiyama Y, Langan P, O'Neill H, Pingali SV, Harton S (2014) Structural coarsening of aspen wood by hydrothermal pretreatment monitored by small- and wide-angle scattering of X-ray and neutrons on oriented specimens. Cellulose 21:1015–1024

Oh SY, Yoo DI, Shin Y, Kim HC, Kim HY, Chung YS, Park WH, Youk JH (2005) Crystalline structure analysis of cellulose treated with sodium hydroxide and carbon dioxide by means of X-ray diffraction and FT-IR spectroscopy. Carbohydr Res 340:2376–2391

Park S, Baker JO, Himmel ME, Parilla PA, Johnson DK (2010) Cellulose crystallinity index: measurement techniques and their impact on interpreting cellulase performance. Biotechnol Biofuels 3:10

Peciulyte A, Karlström K, Larsson PT, Olsson E (2015) Impact of the supramolecular structure of cellulose on the efficiency of enzymatic hydrolysis. Biotechnol Biofuels 8:56

Reiner RS, Rudie AW (2013) Process scale-up of cellulose nanocrystal production to 25 kg per batch at the Forest Products Laboratory. In: Postek MT, Moon RJ, Rudie AJ, Bilodeau MA (eds) Production and applications of cellulose materials. TAPPI Press, Atlanta, pp 21–24

Richter U, Krause T, Schempp W (1991) Untersuchungen zur Alkalibehandlung von Cellulosefasern. Teil 1. Infrarotspektroskopische und Röntgenographische Beurteilung der Ä nderung des Ordnungszustandes. Angew Makromol Chem 185:155–167

R Core Team (2013) R: A language and environment for statistical computing. R Foundation for Statistical Computing, Vienna, Austria. http://www.R-project.org

Schenzel K, Fischer S, Brendler E (2005) New method for determining the degree of cellulose I crystallinity by means of FT Raman spectroscopy. Cellulose 12:223–231

Scherrer P (1918) Bestimmung der Grösse und der inneren Struktur von Kolloidteilchen mittels Röntgenstrahlen. Nachrichten von der Gesellschaft der Wissenschaften, Göttingen, pp 98–100

Segal L, Creely JJ, Martin AE, Conrad CM (1959) An empirical method for estimating the degree of crystallinity of native cellulose using the X-ray diffractometer. Text Res J 29:786–794

Sisson WA (1933) X-ray analysis of fibers, part I, literature survey. Text Res J 3:295–307

Sugino H, Sugimoto H, Miki T, Kanayama K (2007) Fine structure changes of wood during moisture adsorption and desorption process analyzed by X-ray diffraction measurement. Mokuzai Gakkaishi 53:82–89

TAPPI test method (1983) Acid insoluble lignin in wood and pulp; official test method T-222 (Om). TAPPI, Atlanta

Toba K, Yamamoto H, Yoshida M (2013) Crystallization of cellulose microfibrils in wood cell wall by repeated dry-and-wet treatments, using X-ray diffraction technique. Cellulose 20:633–643

Tokoh C, Takabe K, Fujita M, Saiki H (1998) Cellulose synthesized by *Acetobacter xylinum* in the presence of acetyl glucomannan. Cellulose 5:249–261

Vieira FS, Pasquini C (2014) Determination of cellulose crystallinity by terahertz-time domain spectroscopy. Anal Chem 86:3780–3786

Wormald P, Wickholm K, Larsson PT, Iversen T (1996) Conversions between ordered and disordered cellulose. Effects of mechanical treatment followed by cyclic wetting and drying. Cellulose 3:141–152

Zabler S, Paris O, Burgert I, Fratzl P (2010) Moisture changes in the plant cell wall force cellulose crystallites to deform. J Struct Biol 171:133–141

Zhu H, Luo W, Ciesielski PN, Fang Z, Zhu JY, Henriksson G, Himmel ME, Hu L (2016) Wood-derived materials for green electronics, biological devices, and energy applications. Chem Rev 116:9305–9374